SIAM J. IMAGING SCIENCES
Vol. 1, No. 2, pp. 188–208

Combining Image Reconstruction and Image Analysis with an Application to Two-Dimensional Tomography*

Alfred K. Louis†

Abstract. The tasks of image reconstruction from measured data and the analysis of the resulting images are more or less strictly separated. One group of scientists computes by applying reconstruction algorithms to the images; the other then operates on these images to enhance the analysis. First attempts at combining image reconstruction and image analysis, in a nonsystematic way, are known as Lambda tomography or Tikhonov–Phillips methods with ℓ_1-norms or with level-set methods. The aim of this paper is to provide a general tool to combine these two steps; i.e., even in the reconstruction step the future image analysis step is taken into account, leading to a new reconstruction kernel. Here we concentrate on linear methods. As a practical example we consider the image reconstruction problem in computerized tomography followed by an edge detection. We calculate a new reconstruction kernel and present results from simulations.

Key words. image analysis, image reconstruction, approximate inverse

AMS subject classifications. 65R32, 45Q05

DOI. 10.1137/070700863

1. Introduction.

In order to extract information from a given image, analysis tools are used. In a first step one applies operators on that image; then the searched-for information is found by operating on these enhanced versions of the original picture. Images typically are two-dimensional arrays of numbers. Of course, three-dimensional arrays for volume data or even time-dependent data, which may amount to four-dimensional data, are conceivable. Prominent analysis tools are edge detection methods where first partial derivatives of smoothed versions of the image are computed, followed by recognition methods. A typical example is the Canny edge detector; see [4]. Other operations can be found, e.g., in [6, 11]. Here we restrict our discussion, as mentioned above, to linear operators. In denoising one can think of solving the heat equation with homogeneous boundary conditions and the original image as initial condition, at the final time T the image is considered to be denoised.

We have to mention, of course, that nonlinear methods also play an essential role. But this does not—at least at the moment—fit into our framework.

Attempts to combine reconstruction and analysis are known, but are not systematically pursued. As an example we mention the Λ computerized tomography, in which local inversion formulas produce images where the singular support is preserved; this means that those images have jumps wherever the original image has them (see, e.g., [10, 13, 21]). The use of Tikhonov–Phillips regularization with ℓ_1-norms results in smooth images; see, e.g., [5]. Level-set methods

*Received by the editors August 24, 2007; accepted for publication (in revised form) February 19, 2008; published electronically June 11, 2008.
http://www.siam.org/journals/siims/1-2/70086.html

†Department of Applied Mathematics, Saarland University, D-66041 Saarbrücken, Germany (louis@num.uni-sb.de).

in combination with tomography data lead to the determination of the boundary of the object, at least if the object is relatively smooth with jumps along smooth curves; see, e.g., [29]. Another possibility is the direct calculation of wavelet coefficients of the searched-for solution; see [22] and, for an application to tomography, [3, 14]. These coefficients may be used in classification algorithms or in local reconstructions; see [26]. Here, as a mollifier (see next section), we use the scaling function and the wavelets.

In order to make the statements more precise we consider the following example. In computerized tomography the images are produced by applying reconstruction algorithms to the measured data. In this way one calculates images which are smoothed versions of the original density distributions. The result can be presented as

$$f_\gamma = f * e_\gamma =: E_\gamma f,$$

where f is the original object and e_γ is a mollifier depending on the reconstruction method. In the image analysis part, for example, in the above-mentioned edge detection methods, one then computes derivatives of smoothed versions of this image. Typically one calculates in a first step

$$\begin{aligned} f_{\gamma\beta k} &= \frac{\partial}{\partial x_k}(G_\beta * f_\gamma) = \frac{\partial}{\partial x_k}(W_\beta f_\gamma) \\ &= \frac{\partial}{\partial x_k}(W_\beta E_\gamma f), \end{aligned}$$

where G_β represents a mollifier, for example, a Gaussian kernel, and where the two parameters β and γ are chosen independently. The aim of this paper is to provide a method which allows for directly computing in one step the smoothed version of the derivative. To this end in section 2 we generalize the concept of approximate inverse as introduced in [20]. We precompute independently of the data g a reconstruction kernel ψ_γ by solving an auxiliary problem $A^*\psi_\gamma = e_\gamma$. Then the solution is calculated as $g * \psi_\gamma$. A further advantage is that invariances of the operator combined with suitable mollifiers lead to very efficient reconstruction methods.

In section 2 we present some basic facts about linear ill-posed problems, and in section 3 we introduce the approximate inverse for combining the two steps of regularization and analyzing. In section 4 we study the regularization properties of the new method. Section 5 is devoted to the efficient calculation of the result using invariances of the included operators. Finally in the last section we present results for the case of tomography in combination with edge detection, and we derive a new filter and present results from simulations, showing that the results obtained in this way are better than with the classical approach of separately performing reconstruction and differentiation. In addition the computing is much quicker.

2. Linear ill-posed problems. We consider a continuous mapping A between the Hilbert spaces X and Y. The problem (A, X, Y) is called well-posed if $Af = g$ has a unique solution that depends continuously on the data. If one of those conditions is not fulfilled, the problem is called ill-posed. It is important to include the spaces in this definition; then by changing the spaces we may get well-posed problems. The reason for choosing the given spaces is that, on one hand, the data, including the noise, are mostly not smooth enough to choose a smaller

space Y. On the other hand, by selecting a larger space X we may change the concept of solution, including, for example, distributions.

Many integral equations of the first kind lead to compact operators between X and Y, which means that, if the operator does not have finite rank, the range of Y, denoted by $\mathcal{R}(A)$, is not closed, and hence the inverse is not continuous. In order to define solutions for these in the classical sense not necessarily solvable problems, we introduce the pseudoinverse with domain of definition $\mathcal{D}(A^\dagger) = \mathcal{R}(A) \oplus \mathcal{N}(A^*) \subset \overline{\mathcal{R}(A)} \oplus \mathcal{N}(A^*) = Y$ mapping $g \in \mathcal{D}(A^\dagger)$ to the uniquely determined $f \in \mathcal{N}(A)^\perp \subset X$, which solves

$$Af = P_{\overline{\mathcal{R}(A)}} g, \tag{2.1}$$

where $P_{\overline{\mathcal{R}(A)}}$ is the orthogonal projection onto the closure of the range of A. Hence the null-space of the thus defined $A^\dagger$ is $\mathcal{N}(A^\dagger) = \mathcal{N}(A^*)$.

To measure the degree of ill-posedness, which is important in selecting the appropriate regularization, in principle two concepts are used. One is based on the decay of the singular values of the compact operator A; see [17]. Another possibility is to consider the smoothing properties of A as introduced by Natterer (see [24]) if the spaces are based on L_2-spaces. We say that A smoothes α steps in a Sobolev scale if

$$c_1 \|f\|_{H^{-\alpha}} \le \|Af\|_{L_2} \le c_2 \|f\|_{H^{-\alpha}} \tag{2.2}$$

or

$$c_1 \|f\|_{L_2} \le \|Af\|_{H^{\alpha}} \le c_2 \|f\|_{L_2}, \tag{2.3}$$

where the Sobolev norms for functions in $\mathbb{R}^N$ are defined as

$$\|f\|^2_{H^\alpha} = \int_{\mathbb{R}^N} \big(1 + |\xi|^2\big)^\alpha |\hat{f}(\xi)|^2 d\xi \tag{2.4}$$

with the Fourier transform

$$\hat{f}(\xi) = (2\pi)^{-N/2} \int_{\mathbb{R}^N} f(x) \exp\big(-\imath \xi^\top x\big) dx. \tag{2.5}$$

In the case of Fourier integral operators this definition coincides with the fact that the singular values σ_n of A as mapping between L_2-spaces decay like $O(n^{-\alpha})$. We say that the problem (A, L_2, L_2) is ill-posed of order α.

In this paper we use the smoothing properties in Sobolev scales to measure the degree of ill-posedness for spaces $X = L_2(U)$ and $Y = L_2(V)$ for suitable domains U and V.

The theory of regularization is concerned with the definition of solutions for arbitrary data in Y with the additional aspect of balancing the influence of the unavoidable data error against the best possible resolution in the reconstruction. This is achieved by constructing operators $T_\gamma : Y \to X$ with the property that

$$\lim_{\varepsilon \to 0} T_{\gamma(\varepsilon, g^\varepsilon)} g^\varepsilon = A^\dagger g$$

when $g \in \mathcal{D}(A^\dagger)$ and the erroneous data g^ε go to g for $\varepsilon \to 0$.

It is shown in [19] that many of the well-known regularization methods, including the truncated singular value decomposition, the Tikhonov–Phillips method, and iterative methods such as Landweber and CG, as well as their approximate inverses, are of the form

$$T_\gamma = M_\gamma \tilde{A}^\dagger$$

with a smoothing operator M_γ and a suitable continuation of $A^\dagger$ to all of Y. Another possibility is to first smooth the data and then to invert.

In order to extend the operator $A^\dagger$ to all of $Y = \overline{\mathcal{R}(A)} \oplus \mathcal{N}(A^*)$, we define on $\mathcal{N}(A^*)$

$$\tilde{A}^\dagger g = A^\dagger g = 0, \quad g \in \mathcal{N}(A^*).$$

The right-hand side of condition (2.3) says that A maps $L_2(U)$ continuously to $H^\alpha(V) \subset L_2(V)$ for $\alpha > 0$; hence $\mathcal{R}(A) \subset H^\alpha(V) \subset L_2(V)$. The left-hand side of condition (2.2) says that A is continuously invertible from $\mathcal{N}(A)^\perp \subset L_2(V)$ to $H^{-\alpha}(U)$, where the norm of the inverse is bounded by c_1^{-1}. Hence we define $\tilde{A}^\dagger$ on $\overline{\mathcal{R}(A)}$ as this inverse, observing that on $\mathcal{R}(A)$ this coincides with the definition of $A^\dagger$ due to (2.1), and get the following theorem.

Theorem 2.1. *The continuation of the pseudoinverse $A^\dagger$ to all of $Y = L_2(V)$ is a mapping with $\tilde{A}^\dagger : L_2(V) \to H^{-\alpha}(U)$ with $\|\tilde{A}^\dagger\| \le c_1^{-1}$.*

Proof. We decompose $g \in L_2(V)$ into $g = g_1 + g_0$ with $g_1 \in \overline{\mathcal{R}(A)}$ and $g_0 \in \mathcal{N}(A^*)$; then due to the above construction and (2.2) we get

$$\|\tilde{A}^\dagger g\|_{H^{-\alpha}} \le c_1^{-1} \|g_1\|_{L_2} \le c_1^{-1} \|g\|_{L_2},$$

which completes the proof. ∎

If we use differential operators in the image analysis step, then, with the same arguments as above, we consider these operators L as mapping

$$L : \mathcal{D}(L) \subset X \to X$$

in order to not change the space where the solution or the approximate solution is presented. Obviously, differential operators are unbounded mappings when considered as

$$L : \mathcal{D}(L) \subset L_2(U) \to L_2(U).$$

In order to measure the degree of making the functions less smooth, we assume for a $t > 0$ that

$$\|Lf\|_{H^{s-t}} \le c_{L,s} \|f\|_{H^s}; \tag{2.6}$$

i.e., L is a differential operator or a pseudodifferential operator of order t. The problem of determining Lf from $Af = g$ is then ill-posed of order $\alpha+t$, which means that the ill-posedness is enhanced. When first dealing with ill-posed problems one might think that, by choosing the right spaces, the problem becomes well-posed, but this is impossible, as the above discussion shows.

3. Approximate inverse for combining reconstruction and analysis. The motivation for the approximate inverse where the problem $Af = g$ is stably solved by

$$T_\gamma g = \langle g, \psi_\gamma \rangle$$

with a reconstruction kernel fulfilling $A^*\psi_\gamma = e_\gamma$ with a prescribed mollifier e_γ is at least twofold. First, the calculation of those functionals of the solution may be stably achieved, in contrast to the calculation of the solution itself. This was already observed with the Backus–Gilbert method [1]. The method is too time-consuming to evaluate the solution at all points. See also Eckhardt [8] for the calculation of the derivative of the solution. In connection with tomography it was observed by Grünbaum [7] that the filtered backprojection leads to a mollified version of the searched-for solution. For an early application of the calculation of functionals of the solution to partial differential equations, see [15] and the recent paper by Ovall [27].

The second reason for the introduction of the approximate inverse was to derive fast inversion formulas for the case when the same problem has to be solved repeatedly with different right-hand sides, as is the case for such measuring devices as X-ray scanners. Essential for the method to be fast is the selection of the mollifier e_γ according to the invariances of the operator A, as was observed in [17], where applications to some nonlinear problems are also treated. The essential difference from the mollification method of Murio (see, e.g., [23]) is that $f * e_\gamma$ does not replace f in the equation $Af = g$, where in that way the kernel of the integral operator is smoothed, which even amplifies the ill-posedness of the problem.

In this section we generalize the method of the approximate inverse as analyzed in [18]. Let $A : X \to Y$ be a linear operator between the Hilbert spaces X and Y, and let $L : X \to Z$ be a linear, possibly unbounded, operator between the Hilbert spaces X and Z. Typical examples that we have in mind are differential operators where $Z = X$ and $L : X \to X$ is unbounded, or $Z = \ell_2$ when we compute the wavelet coefficients of the solution, or $Z = \mathbb{R}^N$ when we compute N of those coefficients. In the last two cases the operator L is bounded.

In the reconstruction part we have to solve

$$Af = g \tag{3.1}$$

and then we apply the operation L on the so computed solution f for the image analysis.

Now we adapt the concept of approximate inverse, first introduced in [20]. In [8, 18] even derivatives of the solution of $Af = g$ are directly calculated. We now compute instead of Lf an approximation

$$(Lf)_\gamma = \langle Lf, e_\gamma \rangle$$

with a prescribed mollifier $e_\gamma(x, \cdot) \in X$. The value x depends on the application. In the situation $X = L_2(U)$ and $L : X \to X$, $x \in U$ is the reconstruction point where Lf is evaluated. In the wavelet application x is the index of the scaling function or the wavelet coefficient. We formulate in the following theorem the principle of the reconstruction method, and the technical details, as conditions on the mollifier, are treated in the next section.

Theorem 3.1. *Let $e_\gamma(x, \cdot) \in X$ be a suitably chosen mollifier, and let $\psi_\gamma(x, \cdot) \in Y$ be the solution of the auxiliary problem*

$$A^*\psi_\gamma(x, \cdot) = L^*e_\gamma(x, \cdot). \tag{3.2}$$

Then the smoothed version of the image analysis operation is directly computed from the given data g as

$$(Lf)_\gamma(x) = \langle g, \psi_\gamma(x,\cdot)\rangle. \tag{3.3}$$

Proof. We write the smoothed version of the image analysis part as

$$(Lf)_\gamma(x) = \langle Lf, e_\gamma(x,\cdot)\rangle.$$

Now we use the adjoint operator of L and the auxiliary problem to continue:

$$\begin{aligned}(Lf)_\gamma(x) &= \langle f, L^* e_\gamma(x,\cdot)\rangle \\ &= \langle f, A^*\psi_\gamma(x,\cdot)\rangle \\ &= \langle g, \psi_\gamma(x,\cdot)\rangle,\end{aligned}$$

where in the last step we have used the original equation $Af = g$. ∎

We remark that if the auxiliary problem is not solvable, i.e., if L^*e_γ is not in $\mathcal{R}(A^*) \subset \mathcal{N}(A)^\perp$, then we solve the normal equation $AA^*\psi_\gamma = AL^*e_\gamma$, which still leads to a regularized pseudosolution of the problem of finding Lf.

Definition 3.2. *The operator $S_\gamma : Y \to Z$ defined as*

$$S_\gamma g = \langle g, \psi_\gamma(x,\cdot)\rangle \tag{3.4}$$

is called the approximate inverse *of A to compute an approximation of Lf, and ψ_γ is called the* reconstruction kernel.

4. Regularization method. In this section we study the smoothness conditions necessary to guarantee a suitable solution to the whole problem generalizing the results of [19, 12] in the framework of ill-posed problems [9, 17]. Let A be a linear operator between the Hilbert spaces X and Y, and let L be a linear operator between the Hilbert spaces X and Z.

Definition 4.1. *A* regularization *of $A_L^\dagger := LA^\dagger$ for finding the enhanced solution $Lf \in Z$ of $Af = g$ and the application of the image analysis operator L is a family of operators*

$$\{T_\gamma\}_{\gamma>0},\ T_\gamma : Y \to Z$$

with a mapping $\gamma : \mathbb{R}^+ \times Y \to \mathbb{R}^+$ such that for all $g \in \mathcal{D}(A_L^\dagger)$ and for all $g^\epsilon \in Y$ with $\|g - g^\epsilon\| \le \epsilon$ the equality

$$\lim_{\epsilon\to 0, g^\epsilon \to g} T_{\gamma(\epsilon,g^\epsilon)} g^\epsilon = LA^\dagger g$$

holds.

If the operator L is bounded, then clearly any regularization T_γ for $A^\dagger$ leads with LT_γ to a regularization of $LA^\dagger$. Hence we discuss in the following unbounded operators and use the notation introduced in section 2. The problem $(A, L_2(U), L_2(V))$ is ill-posed of order α, and L is a pseudodifferential operator of order t. In this setting the pseudoinverse $\tilde{A}^\dagger$ maps $L_2(V)$ to the space $H^{-\alpha}(U)$ and then L to $H^{-(\alpha+t)}(U)$. This space is too large; hence we need some smoothing operator to come back to $L_2(U)$ from this large space $H^{-(\alpha+t)}(U)$. In the rest of this section the spaces are considered as spaces over U; hence we omit U.

Theorem 4.2. *Let $M_\gamma : H^{-(\alpha+t)} \to L_2$ be a family of linear continuous operators such that*

$$\text{(i)} \quad \|M_\gamma f\|_{L_2} \le c(\gamma)\|f\|_{H^{-(\alpha+t)}} \text{ for all } f \in \mathcal{N}(A)^\perp,$$
$$\text{(ii)} \quad \lim_{\gamma\to 0}\|M_\gamma L f - Lf\| = 0 \text{ for all } f \in \mathcal{N}(A)^\perp.$$

Then $T_\gamma = M_\gamma L\tilde{A}^\dagger$ is a regularization of $A_L^\dagger$ for finding Lf if we chose γ in such a way that $c(\gamma)\varepsilon \to 0$ for $\varepsilon \to 0$.

Proof. Let $g \in \mathcal{D}(A^\dagger)$ and $g^\epsilon \in L_2$ such that $\|g^\epsilon - g\|_{L_2} \le \epsilon$; then we get with $A^\dagger g = \tilde{A}^\dagger g$ for all $g \in \mathcal{D}(A^\dagger)$ that

$$\begin{aligned}
\|T_\gamma g^\epsilon - A_L^\dagger g\| &\le \|T_\gamma(g^\epsilon - g)\| + \|T_\gamma g - A_L^\dagger g\| \\
&= \|M_\gamma L\tilde{A}^\dagger(g^\epsilon - g)\| + \|T_\gamma g - \tilde{A}_L^\dagger g\| \\
&\le c(\gamma)\|L\tilde{A}^\dagger(g^\epsilon - g)\|_{H^{-(\alpha+t)}} + \|M_\gamma L\tilde{A}^\dagger g - L\tilde{A}^\dagger g\| \\
&\le c(\gamma)c_{L,-\alpha}c_1^{-1}\epsilon + \|M_\gamma L\tilde{A}^\dagger g - L\tilde{A}^\dagger g\| \\
&\overset{\epsilon\to 0}{\longrightarrow} 0
\end{aligned}$$

for $\epsilon \to 0$ and γ such that $c(\gamma)\epsilon \to 0$. ∎

We now look for conditions for e_γ from section 3 in order to guarantee that the method presented there is a regularization. The function $e_\gamma(x, y)$ is defined for $x, y \in U$. If we consider a mollifier e_γ of convolution type in $\mathbb{R}^N$, then we can derive the following result. We denote the Fourier transform of e_γ by $\hat{e}_\gamma$.

Theorem 4.3. *Let $e_\gamma(x, y)$ be of convolution type, i.e., $e_\gamma(x, y) = e_\gamma(x - y)$, and let*

$$\text{(i)} \quad (2\pi)^{N/2}\sup_\xi\{(1 + |\xi|^2)^{(\alpha+t)/2}|\hat{e}_\gamma(\xi)|\} \le c(\gamma),$$
$$\text{(ii)} \quad \sup_{\xi\in\mathbb{R}^N}\left(|(2\pi)^{N/2}\hat{e}_\gamma(\xi) - 1|\right) \overset{\gamma\to 0}{\longrightarrow} 0.$$

Then $T_\gamma g(x) = \langle e_\gamma(x, .), L\tilde{A}^\dagger g\rangle$ is a regularization of $A_L^\dagger$ for finding Lf.

Proof. We check the conditions of Theorem 4.2 as follows:

$$\begin{aligned}
\|M_\gamma f\|^2 &= \|\mathcal{F}(M_\gamma f)\|^2 \\
&= (2\pi)^N \int_{\mathbb{R}^N} |\hat{e}_\gamma(\xi)\hat{f}(\xi)|^2 d\xi \\
&= (2\pi)^N \int_{\mathbb{R}^N} (1 + |\xi|^2)^{-(\alpha+t)}(1 + |\xi|^2)^{(\alpha+t)}|\hat{e}_\gamma(\xi)|^2|\hat{f}(\xi)|^2 d\xi \\
&\le \underbrace{(2\pi)^N \sup_\xi\{(1 + |\xi|^2)^{(\alpha+t)/2}|\hat{e}_\gamma(\xi)|\}^2}_{c(\gamma)^2} \|f\|^2_{H^{-(\alpha+t)}},
\end{aligned}$$

which proves part (i) in Theorem 4.2, and

$$\begin{aligned}
\|M_\gamma Lf - Lf\|^2 = \|\mathcal{F}(M_\gamma Lf - Lf)\|^2 &= \int_{\mathbb{R}^N} |(2\pi)^{N/2}\hat{e}_\gamma(\xi) - 1|^2|\widehat{Lf}(\xi)|^2 d\xi \\
&\le \sup_{\xi\in\mathbb{R}^N}\left(|(2\pi)^{N/2}\hat{e}_\gamma(\xi) - 1|\right)\|Lf\|^2_{L_2} \\
&\longrightarrow 0,
\end{aligned}$$

which proves part (ii) in Theorem 4.2. ■

Example. Let $N = 2$, and let e_γ be such that

$$\hat{e}_\gamma(\xi) = (2\pi)^{-1}\operatorname{sinc}\frac{\gamma|\xi|\pi}{2}\chi_{[-1/\gamma,1/\gamma]}(|\xi|)$$

with $\operatorname{sinc} x = \sin x/x$. Checking the conditions of Theorem 4.3, we obtain

$$\text{(i)}\quad (2\pi)^{1/2}\sup_\xi\{(1+|\xi|^2)^{(\alpha+t)/2}|\hat{e}_\gamma(|\xi|)\} = \left(1+\left|\frac{1}{\gamma}\right|^2\right)^{(\alpha+t)/2} = c(\gamma),$$

$$\text{(ii)}\quad \sup_\xi |2\pi\hat{e}_\gamma(\xi) - 1| \to 0 \text{ for } \gamma \to 0,$$

where we have used that $|\operatorname{sinc}(x)| \le 1$ and $\lim_{\gamma\to 0}\operatorname{sinc}(\gamma x) = \operatorname{sinc}(0) = 1$. We also note that $\sup_\xi |\hat{e}(\xi)| \le (2\pi)^{-1}$. Hence $E_\gamma \tilde{A}_L^\dagger$ is a regularization of $A_L^\dagger$.

5. Invariances. The computational efficiency of the approximate inverse depends heavily on the use of invariances. We mention again the reconstruction problem in tomography. If we choose for each reconstruction point x a special mollifier, namely, $e_\gamma(x,\cdot)$, then the reconstruction kernel also depends on x, and the number of values to store is then the number of reconstruction points times the number of data. If we use invariances, for example, translation and rotational invariances of the Radon transform, and we use these invariances to produce the mollifier, we can reduce this number of values to compute and store to just the number of views per direction. The mathematical basis for this can be found in [18]. Here we derive the corresponding result for the combination of reconstruction and image analysis.

Theorem 5.1. *Let $A : X \to Y$ and $L : X \to Z$ be the two operators as above. Let*

$$T_1 : Z \to Z,$$
$$T_2 : X \to X,$$
$$T_3 : Y \to Y$$

be linear operators with

$$L^*T_1 = T_2L^*, \tag{5.1}$$
$$T_2A^* = A^*T_3, \tag{5.2}$$

and let Ψ_γ be the solution of the following auxiliary problem for a general mollifier $E_\gamma \in \mathcal{D}(L^*)$:

$$A^*\Psi_\gamma = L^*E_\gamma. \tag{5.3}$$

Then the solution for the special mollifier

$$e_\gamma = T_1E_\gamma \tag{5.4}$$

is

$$\psi_\gamma = T_3\Psi_\gamma. \tag{5.5}$$

Proof. We start with the right-hand side of the auxiliary problem and use the above relations to get

$$L^* e_\gamma = L^* T_1 E_\gamma = T_2 L^* E_\gamma = T_2 A^* \Psi_\gamma = A^* T_3 \Psi_\gamma;$$

hence $T_3\Psi_\gamma$ solves the auxiliary problem. ∎

As a consequence we observe that the solution for a special mollifier fulfilling the condition $e_\gamma = T_1 E_\gamma$ can be found as

$$\langle f, e_\gamma \rangle = \langle g, T_3 \Psi_\gamma \rangle.$$

If, for example, the operators A and L are of convolution type and if we also choose the mollifier e_γ to be of convolution type, then the mappings T_k are all of translation type, which means that the final reconstruction formula also is of convolution type.

6. Tomography and edge detector. The mathematical model of computerized tomography in two dimensions, for the parallel geometry, is the Radon transform; see, e.g., [25]. It is defined as

$$\mathbf{R} f(\theta, s) = \int_{\mathbb{R}^2} f(x) \delta(s - x^\top \theta) dx,$$

where $\theta \in S^1$ is a unit vector and $s \in \mathbb{R}$.

We consider $\mathbf{R}$ as a mapping

$$\mathbf{R} : L_2(\Omega) \to L_2(S^1 \times \mathbb{R}),$$

where Ω is a bounded domain in $\mathbb{R}^2$. In the notation of section 2 we have $A = \mathbf{R}$, $U = \Omega$, and $V = S^1 \times \mathbb{R}$. The Radon transform has a trivial null-space. The relations (2.2) and (2.3) hold with $\alpha = 1/2$; see [25].

In the following we summarize a few results. The central slice theorem, or projection theorem, is nothing but the formal application of the adjoint operator for fixed direction θ on $\exp(\imath s\sigma)$:

$$\widehat{\mathbf{R} f}(\theta, \sigma) = (2\pi)^{1/2} \hat{f}(\sigma\theta). \tag{6.1}$$

The Radon transform of a derivative is

$$\mathbf{R} \frac{\partial}{\partial x_k} f(\theta, s) = \theta_k \frac{\partial}{\partial s} \mathbf{R} f(\theta, s); \tag{6.2}$$

see, e.g., [25] and generalizations for higher derivatives. The inversion formula for the two-dimensional Radon transform is

$$\mathbf{R}^{-1} = \frac{1}{4\pi} \mathbf{R}^* \mathbf{I}^{-1}, \tag{6.3}$$

where $\mathbf{R}^*$ is the adjoint operator from L_2 to L_2 known as backprojection

$$\mathbf{R}^* g(x) = \int_{S^1} g(\theta, x^\top \theta) d\theta$$

and the Riesz potential $\mathbf{I}^{-1}$ is defined with the Fourier transform

$$\widehat{\mathbf{I}^{-1} g}(\theta, \sigma) = |\sigma| \hat{g}(\theta, \sigma),$$

where the Fourier transform acts on the second variable.

The following invariances are well established for the Radon transform. Consider for $x \in \mathbb{R}^2$ the shift operators $T_2^x f(y) = f(y-x)$ and $T_3^{x^\top\theta} g(\theta, s) = g(\theta, s - x^\top\theta)$; then

$$\mathbf{R}T_2^x = T_3^{x^\top\theta}\mathbf{R}. \tag{6.4}$$

Another couple of intertwining operators is found by rotation. Let Θ be a unitary 2×2 matrix and $D_2^\Theta f(y) = f(\Theta y)$. Then

$$\mathbf{R}D_2^\Theta = D_3^\Theta\mathbf{R}, \tag{6.5}$$

where $D_3^\Theta g(\theta, s) = g(\Theta\theta, s)$. With the $(T\mathbf{R})^* = \mathbf{R}^*T^*$ we get the relations used in Theorem 5.1. These two invariances lead, for a mollifier of convolution type and independent of the directions, i.e., $e_\gamma(x, y) = E_\gamma(\|x-y\|)$, to a reconstruction kernel for determining f of convolution type, independent of the direction, namely, $\psi_\gamma(x;\theta,s) = \Psi_\gamma(s - x^\top\theta)$.

For the edge detectors we use differential operators $\mathbf{L}_k = \frac{\partial}{\partial x_k}$. These operators are considered as

$$\mathbf{L}_k : \mathcal{D}(\mathbf{L}_k) \subset L_2(\Omega) \to L_2(\Omega);$$

hence the scalar products used in the following are L_2 scalar products. They fulfill condition (2.6) with

$$t = 1.$$

We recapitulate the facts necessary to apply the results from the last section. The Radon transform fulfills conditions (2.2) and (2.3) with $\alpha = 1/2$. The range of $\mathbf{R}$ is described by consistency conditions, known as Helgason–Ludwig–Gelfand conditions; for references see, e.g., [25, 28]. The operators $\mathbf{L}_k$ fulfill (2.6) with $t = 1$, which means that the domain of $\mathbf{R}^\dagger_{\mathbf{L}_k}$ consists of those functions in $\mathcal{D}(\mathbf{R}^\dagger)$ such that $\mathbf{R}^\dagger g \in H^1(\Omega)$; hence $\mathbf{L}_k\mathbf{R}^\dagger g \in L_2(\Omega)$. The whole problem of determining $\mathbf{L}_k f$ from $\mathbf{R}f = g$ is thus ill-posed of order

$$\alpha + t = 3/2. \tag{6.6}$$

We observe that $\mathbf{L}_k$ also intertwines with the shift operators considered above. Hence, Theorem 5.1 tells us immediately that if we choose a mollifier of convolution type, then the reconstruction also is of filtered backprojection type as is the case for the standard reconstruction algorithm for determining f. In order to find the dependency of the reconstruction kernel with respect to the direction, we make use of the relation of the Radon transform and the differential operators given in (6.2).

Theorem 6.1. *Let the mollifier $e_\gamma(x,\cdot)$ be given as*

$$e_\gamma(x, y) = E_\gamma(\|x-y\|). \tag{6.7}$$

Then the reconstruction kernel for finding $\mathbf{L}_k f$, where $\mathbf{L}_k = \frac{\partial}{\partial x_k}$, is $\psi_\gamma(x,\cdot)$ with

$$\psi_{\gamma k}(x;\theta,s) = \theta_k \Psi_\gamma(s - x^\top\theta), \tag{6.8}$$

where θ_k is the kth component of θ and where $\Psi_\gamma(s)$ is determined as

$$\Psi_\gamma = -\frac{1}{4\pi}\frac{\partial}{\partial s} I^{-1}\mathbf{R}E_\gamma. \tag{6.9}$$

If, in addition, $\hat{E}_\gamma$ fulfills the conditions of Theorem 4.3, then $S_\gamma g := \langle g, \psi_{\gamma k}\rangle$ is a regularization of $\mathbf{R}^\dagger_{\mathbf{L}_k}$.

Proof. We start with the auxiliary problem and use the inversion formula for $\mathbf{R}$:

$$\begin{aligned}\mathbf{R}^*\psi_\gamma &= \mathbf{L}_k^* e_\gamma \\ &= \mathbf{R}^{-1}\mathbf{R}\mathbf{L}_k^* e_\gamma \\ &= \frac{1}{4\pi}\mathbf{R}^*\mathbf{I}^{-1}\mathbf{R}\mathbf{L}_k^* e_\gamma;\end{aligned}$$

hence we get

$$\psi_\gamma = \frac{1}{4\pi}\mathbf{I}^{-1}\mathbf{R}\mathbf{L}_k^* e_\gamma.$$

The relation (5.2) between Radon transform and differential operators together with $L_k^* = -L_k$ results in

$$\psi_\gamma = -\frac{1}{4\pi}\theta_k \mathbf{I}^{-1}\frac{\partial}{\partial s}\mathbf{R}e_\gamma.$$

Using Fourier transforms we see that I^{-1} and $\frac{\partial}{\partial s}$ commute; hence

$$\psi_\gamma = -\frac{1}{4\pi}\theta_k \frac{\partial}{\partial s}\mathbf{I}^{-1}\mathbf{R}e_\gamma.$$

Now e_γ is independent of a direction, as are $\mathbf{R}e_\gamma$ and the derivatives. Combining this with the conclusions of Theorem 5.1, we prove the above statement. ∎

In the following we present a special mollifier for verifying the theoretical results of the preceding chapters. The cut-off frequency is denoted as b and is related to the γ used before by

$$b = 1/\gamma. \tag{6.10}$$

In a first step we choose the mollifier for the reconstruction part. Because of its advantageous properties we select the mollifier stemming from the Shepp–Logan kernel,

$$\widehat{e_b^1}(\xi) = (2\pi)^{-1}\mathrm{sinc}\frac{\|\xi\|\pi}{2b}\chi_{[-b,b]}(\|\xi\|). \tag{6.11}$$

For the differentiation part we choose with a possibly different parameter β (cf. [16])

$$\widehat{e_\beta^2}(\xi) = (2\pi)^{-1}\mathrm{sinc}\frac{\|\xi\|\pi}{\beta} \tag{6.12}$$

leading to a combined kernel of the form

$$E_{b\beta} = e_b^1 * e_\beta^2 \tag{6.13}$$

with

$$\widehat{E_{b\beta}}(\xi) = (2\pi)^{-1}\operatorname{sinc}\frac{\|\xi\|\pi}{2b}\operatorname{sinc}\frac{\|\xi\|\pi}{\beta}\chi_{[-b,b]}(\|\xi\|). \tag{6.14}$$

Theorem 6.2. *The mollifier $E_{b\beta}$ given in (6.13) is of convolution type and radially symmetric. It fulfills with $\gamma = 1/b$ (see (6.10)) and $\beta = \tau b$*

$$\text{(i)}\quad (2\pi)\sup_{\xi}\{(1+|\xi|^2)^{3/4}|\hat{E}_{b\beta}(\xi)|\} \le c(\gamma) = \left(1+\gamma^{-2}\right)^{3/4},$$

$$\text{(ii)}\quad \sup_{\xi\in\mathbb{R}^2}\left(|(2\pi)^{N/2}\hat{E}_{b\beta}(\xi) - 1|\right) \xrightarrow{\gamma\to 0} 0.$$

Hence, $T_{b\beta}g = \langle g, \psi_{b\beta}\rangle$ with $\psi_{b\beta}$ determined according to Theorem 6.1 is a regularization for determining $\mathbf{L}_k f$, using all the invariances presented in this section.

Proof. Compared to the example at the end of section 4, the Fourier transform of the mollifier $E_{b\beta}$ used here has an additional factor sinc $(\pi\|\xi\|/\beta)$ which is also bounded by 1; hence estimate (i) follows. Due to the fact that the parameter β is tied to b and hence also tends to ∞ for $\gamma \to 0$, this sinc-factor also tends to 1, which proves condition (ii). ∎

In order to compute the reconstruction kernel for determining $L_k f$, we start by computing the Radon transform of $E_{b\beta}$, where we use the fact that the Radon transform of a convolution is the convolution of the Radon transforms

$$\mathbf{R}E_{b\beta} = \mathbf{R}e_b^1 * \mathbf{R}e_\beta^2.$$

Next we use the convolution theorem for Fourier transforms and the projection theorem for the Radon transform to get

$$\begin{aligned}(\mathbf{R}E_{b\beta})\hat{}\,(\sigma) &= (2\pi)^{1/2}(\mathbf{R}e_b^1)\hat{}\,(\sigma)(\mathbf{R}e_\beta^2)\hat{}\,(\sigma)\\ &= (2\pi)^{3/2}\widehat{e_b^1}(\sigma\theta)\widehat{e_\beta^2}(\sigma\theta),\end{aligned}$$

where we use the fact that $E_{b\beta}(x)$ depends only on the length of x; hence its Radon transform is independent of θ, and in the last step we can use any θ. In the following we write, for the sake of simplicity, $e_c(\sigma)$ instead of $e_c(\sigma\theta)$. Now we apply differentiation and the Riesz potential:

$$\begin{aligned}-\frac{1}{4\pi}\left(\frac{\partial}{\partial s}\mathbf{I}^{-1}\mathbf{R}E_{b\beta}\right)\hat{}\,(\sigma) &= -\frac{1}{4\pi}(2\pi)^{3/2}\imath\sigma|\sigma|\widehat{e_\beta^2}(\sigma)\widehat{e_b^1}(\sigma)\\ &= (2\pi)^{1/2}\left(-\imath\sigma(2\pi)^{1/2}\hat{e}_\beta^2(\sigma)\right)\left(\frac{1}{2}(2\pi)^{-1/2}|\sigma|\hat{e}_b^1(\sigma)\right)\\ &= (2\pi)^{1/2}\left(\hat{\psi}_\beta^2(\sigma)\right)\left(\hat{\psi}_b^1(\sigma)\right)\\ &= \left(\psi_\beta^2 * \psi_b^1\right)\hat{}\,(\sigma).\end{aligned}$$

The kernel ψ_b^1 is with the above choice of e_b^1 the Shepp–Logan kernel (see [25, p. 111])

$$\widehat{\psi_b^1}(\sigma) = \frac{1}{8\pi^2}(2\pi)^{1/2}|\sigma|\operatorname{sinc}\frac{\|\xi\|\pi}{2b}\chi_{[-b,b]}(\|\xi\|)$$

with

$$\psi_b^1(s) = \frac{b^2}{2\pi^3} \frac{\frac{\pi}{2} - bs\sin(bs)}{\frac{\pi}{2}^2 - (bs)^2}. \tag{6.15}$$

For the kernel ψ_β^2 we observe that

$$\begin{aligned}
\hat{\psi}_\beta^2(\sigma) &= -\imath\sigma(2\pi)^{-1/2}\mathrm{sinc}\left(\frac{\sigma\pi}{\beta}\right) \\
&= -\imath\sigma(2\pi)^{-1/2}\frac{\sin(\sigma\pi/\beta)}{\sigma\pi/\beta} \\
&= -\imath\frac{\beta}{\pi}(2\pi)^{-1/2}\frac{1}{2\imath}\left(\exp\left(\frac{\imath\sigma\pi}{\beta}\right) - \exp\left(\frac{-\imath\sigma\pi}{\beta}\right)\right) \\
&= -\frac{\beta}{2\pi}\left(\hat{\delta}_{-\pi/\beta} - \hat{\delta}_{\pi/\beta}\right)(\sigma),
\end{aligned}$$

where we used in the last step that

$$\hat{\delta}_s(\sigma) = (2\pi)^{-1/2}\exp(-\imath s\sigma).$$

For the final result of $\psi_{b\beta}$ we then get

$$\begin{aligned}
\psi_{b\beta}(s) &= \psi_\beta^2 * \psi_b^1(s) \\
&= \frac{\beta}{2\pi}\left(\psi_b^1\left(s + \frac{\pi}{\beta}\right) - \psi_b^1\left(s - \frac{\pi}{\beta}\right)\right).
\end{aligned}$$

Now we choose $b = \beta$, which means $\tau = 1$ in the last theorem, and, as usual (see again [25]), we put $b = \pi/h$ and $s_\ell = \ell h$ and get the new filter

$$\psi_{\pi/h}(s_\ell) = \frac{1}{\pi^2 h^3}\frac{8\ell}{\left(3 + 4\ell^2\right)^2 - 64\ell^2}, \quad \ell \in Z. \tag{6.16}$$

To present the algorithm we assume that the data $\mathbf{R}f(\theta, s)$ are given for $s_k = kh$, $k = -q, \ldots, q$, $h = 1/q$, and $\theta_j = (\cos\varphi_j, \sin\varphi_j)^\top$ with $\varphi_j = \pi(j-1)/p$, $j = 1, \ldots, p$.

We choose

$$b = \frac{\pi}{h}, \tag{6.17}$$

leading to the filter ψ_γ from above.

Step 1. For $j = 1, \ldots, p$, evaluate the discrete convolutions

$$v_{m,j} = h\sum_{\ell=-q}^{q} \psi_b(s_j - s_\ell)\mathbf{R}f(\theta_m, s_\ell), \quad j = -q, \ldots, q. \tag{6.18}$$

Step 2. To get the partial derivatives with respect to x_k, $k = 1, 2$, calculate

$$v_{m,j}^k = \theta_{m,k} v_{m,j}. \tag{6.19}$$

Step 3. For each reconstruction point x compute the discrete backprojection

$$\left(\frac{\partial}{\partial x_k} f\right)_b (x) = \frac{2\pi}{p} \sum_{m=1}^{p} \Big((1-\eta) v_{m\ell}^k + \eta v_{m,\ell+1}^k \Big), \tag{6.20}$$

where, for each m and x, ℓ and η are determined by

$$s = \theta^\top x, \quad \ell \le s/h < \ell + 1, \quad \eta = s/h - \ell.$$

When comparing to the standard reconstruction (see, e.g., [25]), we observe that the filter changes and, in addition, we have Step 2, the multiplication with $\cos\varphi_m$ or $\sin\varphi_m$, respectively. The filter is the same for both derivatives.

Here we optimize the choice of the different filters and the selection of the parameters. In order to test the algorithm we choose the well-known Shepp–Logan phantom, where we use the densities originally given by Shepp–Logan; i.e., the skull has the value 2, and the brain has the value 1 (in contrast to the work of many authors, where these values are lowered by 1 leading to a brain consisting of air, as in the outside of the skull). The objects inside the brain differ by 1% up to 3% from the surrounding tissue.

The number of data is $p = 720$ and $q \approx p/\pi$, namely, $q = 326$ leading to 653 rays per view. The reconstruction is computed on a 1025×1025 grid.

Figures 1 and 2 show the result of the above-mentioned algorithm with exact data. We observe that even the height of the jumps is correctly computed within the numerical approximation of the derivatives.

Then we add to the data 5% noise. Figure 3 shows the density reconstruction and Figure 4 the application of the smoothed derivative in the x_1-direction. Figures 5 and 6 show the result of the above algorithm; the contours of the object are clearly visible, which is even the case for the objects differing by only 1% relative to the surrounding tissue. This is not the case for the classical approach in Figure 4 and also not the case for the application of Λ tomography, where the second derivative of the data is computed and backprojected; see Figure 7.

The artifacts outside the object can easily be removed by implementing the support theorem for the Radon transform stating that the object vanishes on lines parallel to θ not meeting the support of the data; see [2].

Figure 8 shows that if we do not follow the theoretically motivated strategy of parameter selection as above we get much worse reconstructions. If we choose a smaller γ, then we lose resolution. As a consequence we note that it pays to combine the two steps of image reconstruction and image analysis wherever possible.

Finally, Figures 9 and 10 show $|\mathbf{L}_1 f| + |\mathbf{L}_2 f|$, where the colortable is changed such that the highest values are black, and the same window is used for both images. Figure 9 is produced with the method presented here, and Figure 10 with first reconstructing f and then performing the differentiation on the smoothed reconstructions as in Figure 4.

Where the computation time is concerned, this approach differs only by the filter selection from the standard filtered backprojection, so it is as fast as this, and the additional computing time for the differentiation of the reconstruction is not needed. When taking into account that the backprojection step in the calculation is due to the determination of which detector

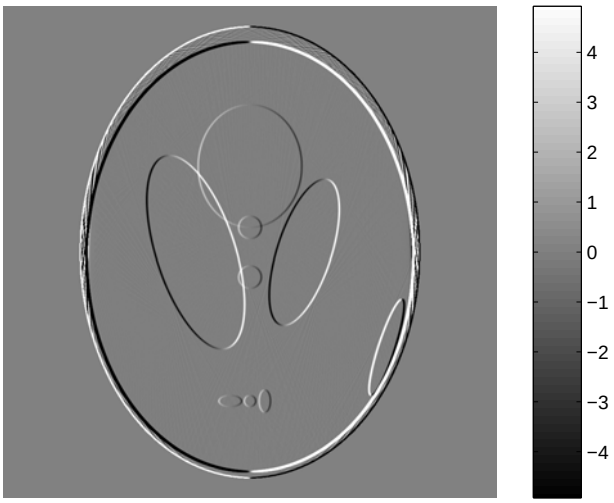

Figure 1. *Application of the above algorithm for the derivative in the x_1-direction with exact data.*

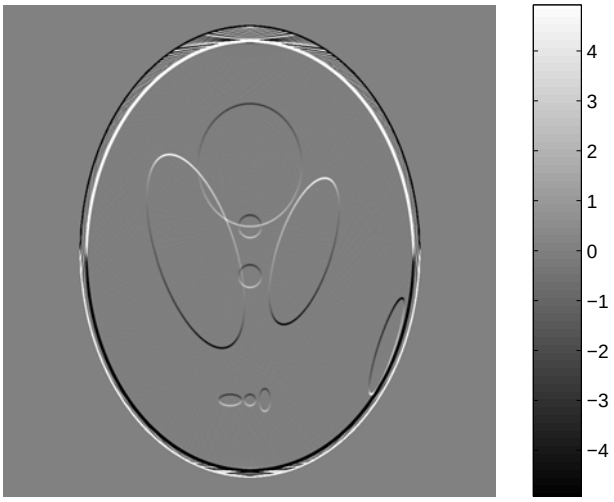

Figure 2. *Application of the above algorithm for the derivative in the x_2-direction with exact data.*

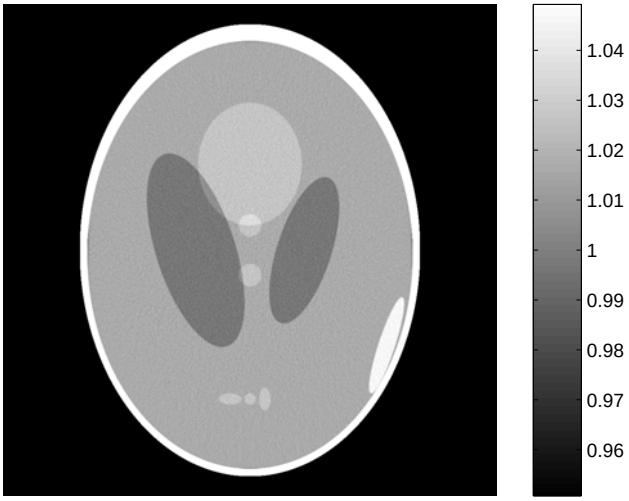

Figure 3. *Classical reconstruction of noisy data.*

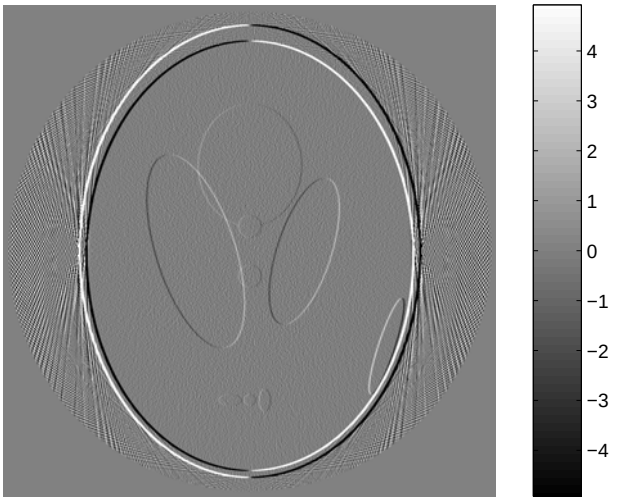

Figure 4. *Smoothed derivative in the x_1-direction of the image in Figure 3.*

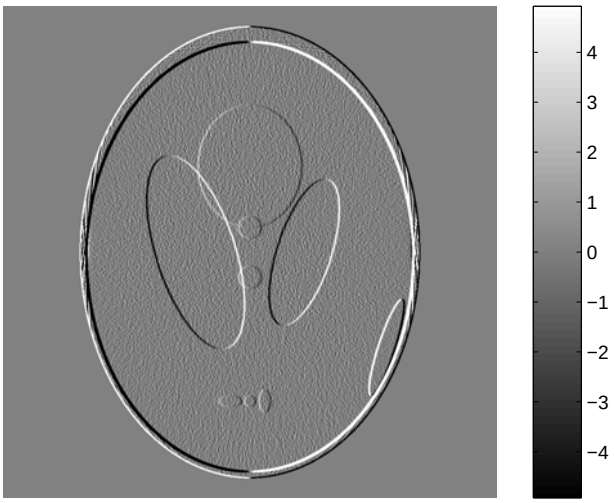

Figure 5. *Application of the above algorithm for the direct computation of the derivative in the x_1-direction.*

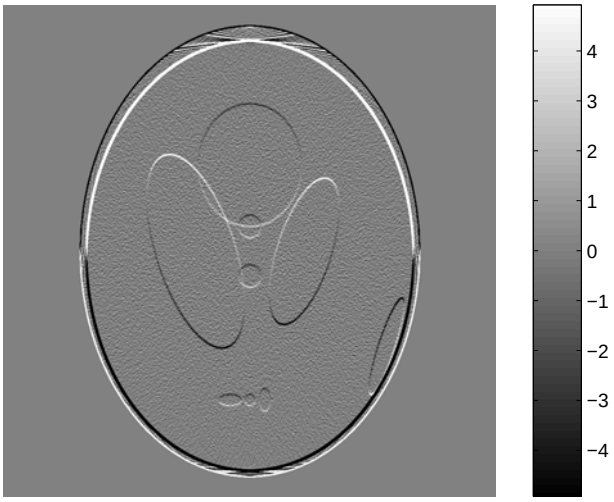

Figure 6. *Application of the above algorithm for the direct computation of the derivative in the x_2-direction.*

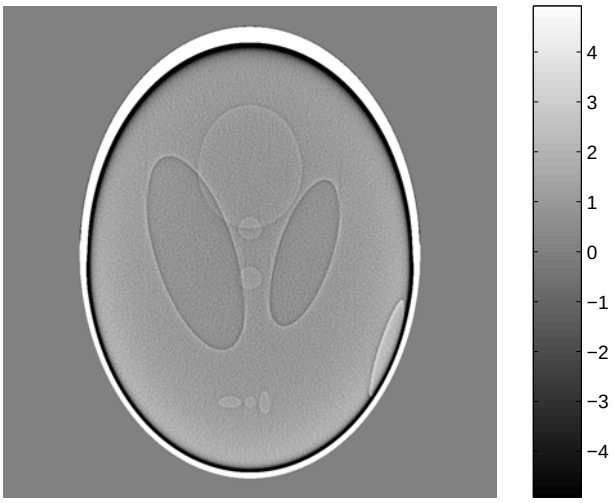

Figure 7. Λ *tomography* [10].

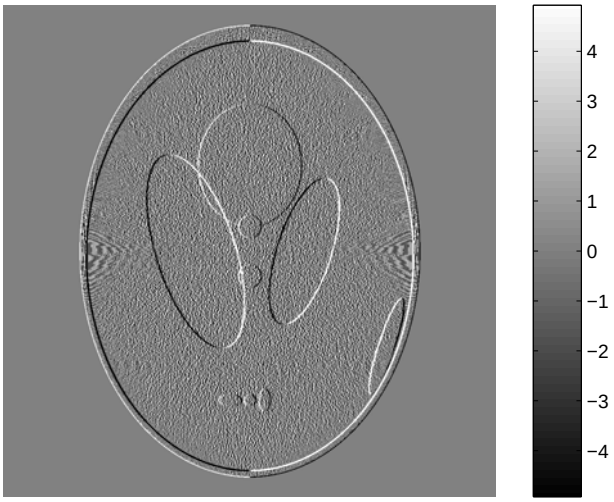

Figure 8. *Reconstruction of the same data set with* $\beta = b$ *replaced by* $\beta = 2b$ *in the second filter.*

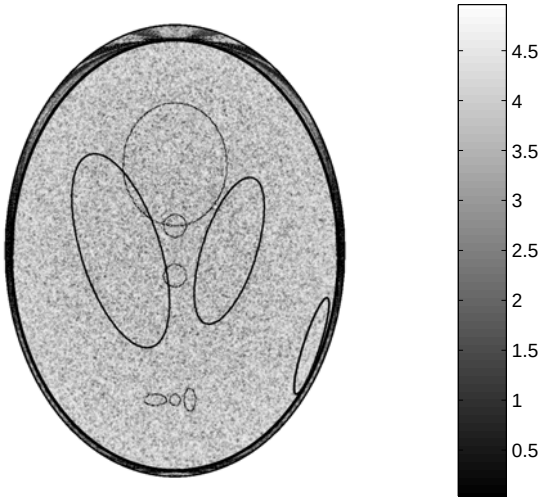

Figure 9. *Display of* $|\mathbf{L}_1 f| + |\mathbf{L}_2 f|$ *with the method presented here.*

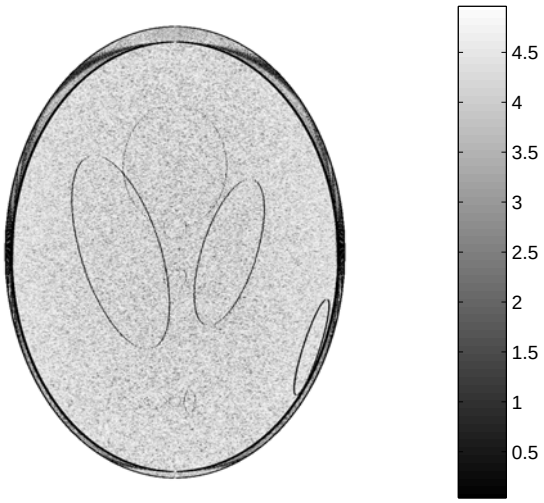

Figure 10. *Display of* $|\mathbf{L}_1 f| + |\mathbf{L}_2 f|$ *when first the function is reconstructed and then the derivatives are computed from the smoothed image; compare to Figure* 4.

position is to be used for a combination of direction and reconstruction points, even the calculation of three images, namely, the density itself and the two derivatives, is almost as fast as the reconstruction of the image itself if it is performed in one program.

REFERENCES

[1] G. Backus and F. Gilbert, *The resolving power of growth earth data*, Geophys. J. Roy. Astron. Soc., 16 (1968), pp. 169–205.

[2] J. Boman and E. T. Quinto, *Support theorems for real analytic Radon transforms*, Duke Math. J., 55 (1987), pp. 943–948.

[3] S. Bonnet, F. Peyrin, F. Turjman, and R. Prost, *Multiresolution reconstruction in fan-beam tomography*, IEEE Trans. Image Process., 11 (2002), pp. 169–176.

[4] J. F. Canny, *A computational approach to edge detection*, IEEE Trans. Pattern Anal. Mach. Intell., 8 (1986), pp. 679–698.

[5] M. Cetin and W. C. Karl, *Feature-enhanced synthetic aperture radar image formation based on nonquadratic regularization*, IEEE Trans. Image Process., 10 (2001) pp. 623–631.

[6] B. Chalmond, *Modeling and Inverse Problems in Image Analysis*, Springer, Berlin, 2003.

[7] M. E. Davison and F. A. Grünbaum, *Tomographic reconstruction with arbitrary directions*, Comm. Pure Appl. Math., 34 (1981), pp. 77–119.

[8] U. Eckhardt, *Zur numerischen Behandlung inkorrekt gestellter Aufgaben*, Computing, 17 (1976/77), pp. 193–206.

[9] H. W. Engl, M. Hanke, and A. Neubauer, *Regularization of Inverse Problems*, Kluwer Academic Publishers, Dordrecht, The Netherlands, 1996.

[10] A. Faridani, D. V. Finch, E. L. Ritman, and K. T. Smith, *Local tomography* II, SIAM J. Appl. Math., 57 (1997), pp. 1095–1127.

[11] B. Jähne, *Handbook of Digital Image Processing for Scientific and Technical Applications*, 2nd ed., CRC Press, Boca Raton, FL, 2004.

[12] P. Jonas and A. K. Louis, *A Sobolev space analysis of linear regularization methods for ill-posed problems*, J. Inverse Ill-Posed Probl., 9 (2001), pp. 59–74.

[13] A. Katsevich, *Improved cone beam local tomography*, Inverse Problems, 22 (2006), pp. 627–643.

[14] I. Loris, G. Nolet, I. Daubechies, and F. A. Dahlen, *Tomographic inversion using ℓ_1-norm regularization of wavelet coefficients*, Geophys. J. Internat., 170 (2007), pp. 359–370.

[15] A. K. Louis, *Acceleration of convergence for finite element solutions of the Poisson equation*, Numer. Math., 33 (1979), pp. 43–53.

[16] A. K. Louis, *Approximate inverse of the 3D Radon transform*, Math. Methods Appl. Sci., 5 (1983), pp. 176–185.

[17] A. K. Louis, *Inverse und schlecht gestellte Probleme*, Teubner, Stuttgart, Germany, 1989.

[18] A. K. Louis, *Approximate inverse for linear and some nonlinear problems*, Inverse Problems, 12 (1996), pp. 175-190.

[19] A. K. Louis, *A unified approach to regularization methods for linear ill-posed problems*, Inverse Problems, 15 (1999), pp. 489–498.

[20] A. K. Louis and P. Maass, *A mollifier method for linear operator equations of the first kind*, Inverse Problems, 6 (1990), pp. 427–440.

[21] A. K. Louis and P. Maass, *Contour reconstruction in 3-D X-Ray CT*, IEEE Trans. Med. Imaging, 12 (1993), pp. 764–769.

[22] A. K. Louis, P. Maass, and A. Rieder, *Wavelets*, 2nd ed., Teubner, Stuttgart, Germany, 1998 (in German); Wiley, Chichester, UK, 1997 (in English).

[23] D. A. Murio, *The Mollification Method and the Numerical Solution of Ill-Posed Problems*, Wiley, Chichester, UK, 1993.

[24] F. Natterer, *Error bounds for Tikhonov regularization in Hilbert spaces*, Appl. Anal., 18 (1984), pp. 29–37.

[25] F. Natterer, *The Mathematics of Computerized Tomography*, Teubner, Stuttgart, Germany, Wiley, Chichester, UK, 1986.

[26] S. Oeckl, T. Schön, A. Knauf, and A. K. Louis, *Multiresolution 3D-computerized tomography and its application to NDT*, in Proceedings of the Ninth European Conference on Non-Destructive Testing (ECNDT), Berlin, 2006.

[27] J. S. Ovall, *Asymptotically exact functional error estimates on superconvergent gradient recovery*, Numer. Math., 102 (2006), pp. 543–558.

[28] E. T. Quinto, *Radon transforms, differential equations, and microlocal analysis*, in Radon Transforms and Tomography, Contemp. Math. 278, AMS, Providence, RI, 2001, pp. 57-68.

[29] R. Ramlau and W. Ring, *A Mumford-Shah level-set approach for the inversion and segmentation of X-ray tomography data*, J. Comput. Phys., 221 (2007), pp. 539–557.